

RESEARCH ARTICLE

A population Monte Carlo model for underwater acoustic telemetry positioning in reflective environments

James Adam Campbell¹  | Samuel Joseph Shry² | Petter Lundberg³  | Olle Calles² | Franz Hölker¹

¹Community and Ecosystem Ecology, Leibniz Institute of Freshwater Ecology and Inland Fisheries (IGB), Berlin, Germany

²River Ecology and Management Research Group RivEM, Department of Environmental and Life Sciences, Karlstad University, Karlstad, Sweden

³Department of Wildlife, Fish and Environmental Studies, Swedish University of Agricultural Sciences, Umeå, Sweden

Correspondence

James Adam Campbell
Email: jamesadamcampbell@gmail.com

Funding information

Stiftelsen för Kunnaps- och Kompetensutveckling, Grant/Award Number: 20160160; LIFE Programme, Grant/Award Number: LIFE18 NAT/SE/000742; H2020 Marie Skłodowska-Curie Actions, Grant/Award Number: 860800; Uniper/Sydkraft Hydropower AB

Handling Editor: Chloe Victoria Robinson

Abstract

1. Underwater acoustic telemetry positioning is widely used to track the fine-scale movements of aquatic animals. In study areas near acoustically reflective surfaces, reflected transmissions may cause large detection outliers that can severely reduce the accuracy of positioning models.
2. A novel time-of-arrival model for telemetry positioning is presented that utilizes a population Monte Carlo algorithm to solve positions (termed PMC-TOA). Telemetry detection error is modelled as a mixture distribution, allowing reflected detections to be identified and positions to be estimated despite their presence. Importantly, the PMC-TOA model provides good measures of positioning uncertainty, facilitating the use of post-processing state-space models to further refine position estimates.
3. A simulated telemetry study is used to validate the PMC-TOA model and compare its performance to a conventional time-difference-of-arrival positioning model. A real case study on Atlantic salmon (*Salmo salar*) smolt passage behaviour is further used to demonstrate how PMC-TOA can be combined with post-processing models to produce high-resolution tracks. The resulting tracks are compared against those resulting from YAPS and TDOA positioning.
4. The PMC-TOA model was shown to work well as either (i) a pre-processing step to remove reflected transmissions from time-of-arrival datasets, or (ii) a fast and accurate positioning method when paired with a post-processing state-space model. Positions returned by the model can be further used for animal movement statistics, allowing researchers to test the effects of experimental or environmental factors on the fine-scaled movement behaviours of aquatic animals in acoustically challenging environments.

KEYWORDS

acoustic telemetry, animal movement statistics, aquatic tracking, movement ecology, population Monte Carlo, telemetry tracking, time-of-arrival positioning

This is an open access article under the terms of the [Creative Commons Attribution](https://creativecommons.org/licenses/by/4.0/) License, which permits use, distribution and reproduction in any medium, provided the original work is properly cited.

© 2025 The Author(s). *Methods in Ecology and Evolution* published by John Wiley & Sons Ltd on behalf of British Ecological Society.

1 | INTRODUCTION

Acoustic telemetry has recently become a standard method for tracking aquatic animals in their natural environment (Lennox et al., 2023). As the water surface and bottom substrate—when below the critical grazing angle—are effectively acoustic mirrors, the water column can act as a waveguide that allows sound to propagate over far distances (see Ainslie, 2010; Bucker, 1964). When background noise levels are low, acoustic telemetry receivers can be effective at detecting passing animals tagged with transmitters.

In addition to presence/absence surveys, acoustic telemetry is also used for 2- or 3-dimensional positioning of animals passing through arrays of receivers. Here, time-difference-of-arrival (TDOA) methods (see Smith & Abel, 1987)—commonly used by commercial positioning services (Lennox et al., 2023)—can estimate the point position of the tagged animal during an emission event. Furthermore, if reasonable assumptions can be made about the animal's underlying movement process, time-of-arrival state-space models (such as YAPS; Baktoft et al., 2017) can be employed for track positioning. Utilizing a joint likelihood function comprised of a time-of-arrival (observation) and some type of random walk (process) model, state-space positioning can give location estimates far more precise than those resulting from TDOA methods (Vergeynst et al., 2020).

In the aforementioned methods, tag transmissions are assumed to propagate directly between the tag and the receiver. However, fish behavioural studies are often located in areas near acoustically reflective structures such as dams, weirs, canal walls, fish passes, etc. (see Ingraham et al., 2014; Kjærås et al., 2023; Trancart et al., 2020). Those transmissions that reflect off these structures can result in large positive outliers for positioning models—tag detections occurring far later than they are expected. Unless these detections are removed beforehand or the model is explicitly designed to handle such cases, the resulting positioning accuracy can be poor.

This paper introduces a time-of-arrival positioning model fitted using population Monte Carlo (hereafter referred to as PMC-TOA positioning). It is designed to identify reflected transmissions and solve positions despite their presence. The resulting positions and their covariances can then be passed on to animal movement state-space models for post-processing. Alternatively, this model can be used as a pre-processing step, removing likely reflected detections from time-of-arrival data that can then be used by other positioning models. So long as suitable parameters for the study site are chosen, PMC-TOA presents a fast method for point estimation and identification of reflections.

Following the description of PMC-TOA, data from simulated and real case studies containing reflected telemetry detections will be used to compare the performance of the proposed model to conventional TDOA positioning. The real case study will exemplify how PMC-TOA can be combined with a post-processing state-space model for robust track positioning of fish, and the resulting tracks will be compared to those from YAPS.

2 | METHODS

The source code for PMC-TOA, TDOA, and the continuous-time correlated random walk models used in the following sections—along with reproducible examples of their application to the case study data—has been provided as [Supporting Information](#).

2.1 | Population Monte Carlo positioning

Population Monte Carlo (PMC) is a class of algorithms for estimating target distributions that is based on adaptive importance sampling (Cappé et al., 2004). Broadly, PMC algorithms iteratively adapt one or more proposal distribution(s) to match an unknown target distribution of, in our case, the likely time and location of a tag emission. On each iteration, sets of parameter values—particles—are sampled from the proposal densities. Here, a particle holds a plausible time and position of an emission event. Through importance weighting and then resampling of these particles using time-of-arrival measurements, the proposal distributions are updated on each iteration to more closely match the target distribution. After a fixed number of iterations, the weighted particles are returned as an approximation to the target distribution, thus providing the position estimate.

PMC-TOA utilizes the deterministic mixture PMC algorithm presented in Elvira et al. (2017) and is as follows:

1. Initialization

A set of N proposal distributions are generated. These are a set of multivariate Gaussian distributions, q , centred on $\mathbf{M}^{(1)} = \{\mu_1^{(1)}, \dots, \mu_N^{(1)}\}$ with a fixed covariance of Σ_{prop} . The vector of measured detection times on K receivers for a single tag emission is stored as $\mathbf{y} = (y_1, \dots, y_K)$.

2. for $g = 1$ to G

a. Sample a particle from each proposal distribution

$$\mathbf{x}_i^{(g)} \sim q(\mu_i^{(g)}). \quad (1)$$

Each particle is a vector that holds the spatial coordinates and time of a proposed tag emission event. The set of all particles for this iteration is represented by $\mathbf{X}^{(g)} = \{\mathbf{x}_1^{(g)}, \dots, \mathbf{x}_N^{(g)}\}$.

b. Calculate the importance weights for the sampled particles with

$$w_i^{(g)} = \frac{\mathcal{L}(\mathbf{x}_i^{(g)} | \mathbf{y})}{N^{-1} \cdot \sum_{j=1}^N q(\mathbf{x}_j^{(g)} | \mu_j^{(g)})} \quad (2)$$

(for $i = 1, \dots, N$), where $\mathcal{L}(\mathbf{x}_i^{(g)} | \mathbf{y})$ is the time-of-arrival likelihood and $q(\mathbf{x}_i^{(g)} | \mu_j^{(g)})$ is the proposal density. The denominator causes particles located in more densely sampled areas to receive lower weights, facilitating exploration of the sample space. Next, normalize these weights with

$$\bar{w}_i^{(g)} = \frac{w_i^{(g)}}{\sum_{j=1}^N w_j^{(g)}}. \quad (3)$$

The vector of weights for this iteration is then $\bar{\mathbf{w}}^{(g)} = (\bar{w}_1^{(g)}, \dots, \bar{w}_N^{(g)})$.

- c. Update the proposal location parameters for the next iteration $\mathbf{M}^{(g+1)}$ by resampling with replacement from the particles $\mathbf{X}^{(g)}$ using the weights $\bar{\mathbf{w}}^{(g)}$.

3. Output

Return the set of particles and weights from the final iteration $\mathbf{X}^{(G)}$ and $\bar{\mathbf{w}}^{(G)}$.

After running the above algorithm for a fixed number of iterations, the distribution of weighted particles should provide an approximation to the time-of-arrival likelihood, $\mathcal{L}(\mathbf{x}_i^{(g)} | \mathbf{y})$. The estimate and covariance of the most likely tag position and emission time can then be taken from the weighted mean and covariance of these particles.

The time-of-arrival likelihood for a given particle is calculated by first getting the detection error—the measured minus expected detection times across the array, given by

$$\epsilon(\mathbf{x}_i, \mathbf{r}_k) = y_k - (c^{-1} \cdot \|\mathbf{s}_i - \mathbf{r}_k\| + m_i). \quad (4)$$

The tag coordinates are given by the vector $\mathbf{s}_i = (s_{ix}, s_{iy})$ and the emission time is m_i . Particles are then vectors taking the form $\mathbf{x}_i = (s_{ix}, s_{iy}, m_i)$. The coordinates of receiver k are stored in the vector \mathbf{r}_k and c gives the speed of signal transmission. The time-of-arrival likelihood is then treated as a mixture distribution,

$$\mathcal{L}(\mathbf{x}_i^{(g)} | \mathbf{y}) = \prod_{k=1}^K \left[\frac{1}{2} \cdot f_{\text{drct}}(\epsilon(\mathbf{x}_i^{(g)}, \mathbf{r}_k)) + \frac{1}{2} \cdot f_{\text{refl}}(\epsilon(\mathbf{x}_i^{(g)}, \mathbf{r}_k)) \right]. \quad (5)$$

$f_{\text{drct}}(\epsilon(\mathbf{x}_i^{(g)}, \mathbf{r}_k))$ is a Gaussian density with a mean of zero and a standard deviation of σ_{det} . This component aims to capture the relatively small detection error expected from direct tag transmissions. $f_{\text{refl}}(\epsilon(\mathbf{x}_i^{(g)}, \mathbf{r}_k))$ is a generalized normal distribution from Nadarajah (2005) with location and scale parameters both set to $0.5 \cdot \phi$ and a shape parameter, β , set to some high value. As β increases, the density function more closely approximates a uniform distribution spanning zero to ϕ , where ϕ gives the maximum expected error resulting from a reflected detection. This component captures large positive outliers resulting from reflections. Figure 1 provides a visualization of the component densities which make up this likelihood function. As the component densities are equally weighted, the likelihood function treats each detection as having an equal probability of being either a reflected or direct transmission.

For the multivariate Gaussian proposal distribution, the covariance matrix can be set to

$$\Sigma_{\text{prop}} = \begin{bmatrix} c^2 \sigma_{\text{prop}}^2 & 0 & 0 \\ 0 & c^2 \sigma_{\text{prop}}^2 & 0 \\ 0 & 0 & \sigma_{\text{prop}}^2 \end{bmatrix}, \quad (6)$$

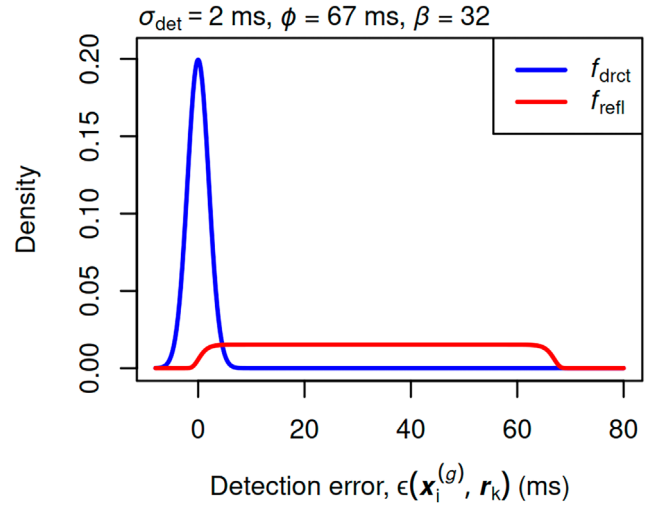


FIGURE 1 An illustration of the direct and reflected probability density functions that make up the time-of-arrival likelihood. Direct transmissions are assigned a small Gaussian error, while reflected transmissions are modelled as an approximation to a uniform distribution that captures large positive outliers caused by late-arriving reflections.

where σ_{prop} is a standard deviation parameter. The first two diagonal entries give the spatial variance along the axes holding the tag coordinates (for the respective x and y dimensions) and the third is the emission time variance. σ_{prop} should be given a value greater than σ_{det} to avoid sample impoverishment—particles getting ‘stuck’ in a small area of the sample space.

Using the final set of particles and weights, the probability that a given detection, y_k , resulted from a reflected transmission is given by

$$p_k(y_k | \mathbf{X}^{(G)}) = \sum_{i=1}^N \bar{w}_i \cdot \frac{f_{\text{refl}}(\epsilon(\mathbf{x}_i^{(g)}, \mathbf{r}_k))}{f_{\text{drct}}(\epsilon(\mathbf{x}_i^{(g)}, \mathbf{r}_k)) + f_{\text{refl}}(\epsilon(\mathbf{x}_i^{(g)}, \mathbf{r}_k))}. \quad (7)$$

For classification purposes, likely reflections can be marked when the probability of a reflected transmission exceeds some threshold value, $p_k(y_k | \mathbf{X}^{(G)}) \geq p_{\text{thresh}}$. The choice of threshold value here depends on the desired sensitivity of the classifications.

Lastly, the initial set of location parameters for the proposal densities, $\mathbf{M}^{(1)}$, can have a large impact on the performance of the algorithm. Each $\mu_i^{(1)}$ consists of the possible spatial location and time of a tag emission. The tag coordinate for each initial location parameter, $\mathbf{s}_i^{(1)}$, can be uniformly sampled from a polygon surrounding the receiver array, covering the whole area where tag emissions are expected to be detected. Per each sampled location, $\mathbf{s}_i^{(1)}$ and \mathbf{y} can then be passed to Equation (4). Assuming detections result from direct transmissions where $\epsilon(\mathbf{x}_i^{(1)}, \mathbf{r}_k) = 0$ s, the emission time, $m_i^{(1)}$, can be solved for on each receiver. Across receivers, the earliest of these emission time estimates can be used for the location parameter, $\mu_i^{(1)} = (s_{ix}^{(1)}, s_{iy}^{(1)}, m_i^{(1)})$, as later values may result from reflected transmissions.



FIGURE 2 A satellite image of the study area used in both the simulated and real case studies. Downstream migrating smolts—swimming southward—can choose one of two routes passing the study area: (i) through the opening in the spillway or (ii) enter the hydropower turbine intake channel. The receiver array was set up to observe this route choice behaviour. Coordinate reference system: WGS84/UTM Zone 33N. Attribution: Imagery ©2025 Airbus, Lantmäteriet/Metria, Maxar Technologies, Map data ©2025.

2.2 | Simulated study

PMC-TOA was validated by comparing its performance to a conventional TDOA algorithm in a simulated arena. The arena held an array of six telemetry receivers, and tag emission events were simulated at random locations within the space. For each emission event, five receivers would detect either a direct or reflected transmission, and one receiver would always have a missed detection. The geometry and receiver array configuration were taken from a real study that aimed to track Atlantic salmon smolt passage at a hydropower spillway located along the river Mörrumsån, Sweden (Figure 2). The spillway (south-eastward) and fish pass (eastward) were designated as acoustically reflective surfaces.

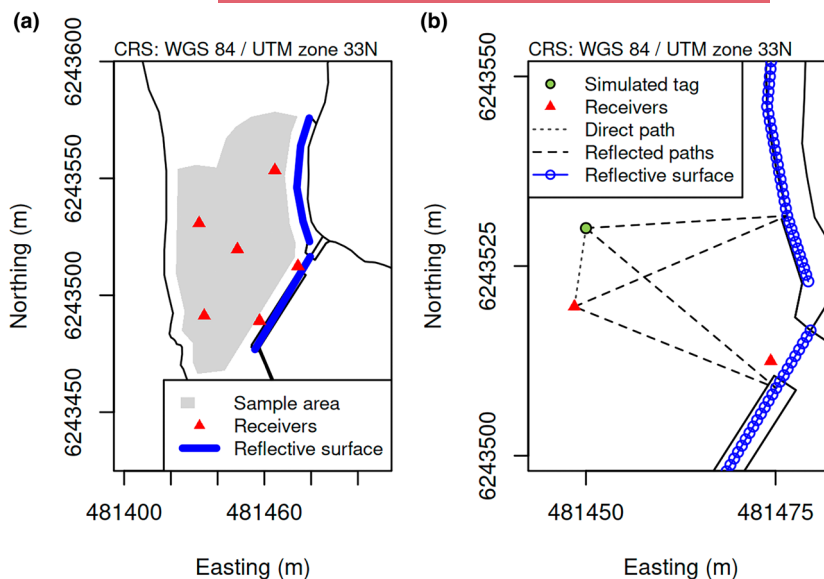
Five hundred tag positions were randomly sampled from the study area shown in Figure 3, with emission times fixed at 0s. Four time-of-arrival datasets were then generated from those tag positions, containing 0, 1, 2, and 3 reflected detections per emission, resulting in a total of 2000 simulated emissions.

For each tag location: using a transmission velocity of 1500 ms^{-1} , the expected detection times were calculated for each receiver resulting from direct transmissions. Array receivers with valid

reflection geometries were then identified. Of these, a number of them were randomly selected to record a detection time resulting from a reflected transmission. If the tag and receiver geometry was such that a transmission could have reflected off either the spillway or the fishpass, one of these was randomly selected as the reflected transmission path. For the remaining receivers detecting direct transmissions, one receiver was randomly selected to have a missed detection. This resulted in a total of five out of six receivers detecting either a direct or reflected transmission per emission event. Finally, additional detection error was added to all receivers by sampling from a Gaussian with a mean of 0s and standard deviation of 2ms, selected to roughly replicate the distribution of observed detection error at this study site.

The reflection geometry—the path of the reflected transmissions—was calculated by drawing a transect of points along a given reflection surface. These points were evenly spaced approximately 1m apart. Each transect point was then evaluated to check if a transmission could have reflected from that location: if the angles of incidence and reflection at that point were similar. The point along the transect with the smallest difference between these angles was taken as the reflected path, given that difference was smaller than 5° . If the minimum difference in angles was larger than 5° , this was taken as the surface

FIGURE 3 (a) The area of river used in the simulated study, bounded by the black outline. Blue lines are reflective surfaces (a fish pass and spillway) which tag transmissions may reflect off. The grey polygon shows the area where simulated tag locations are randomly sampled from and red triangles are the receiver locations. (b) An example simulated tag, along with two valid transmission reflection geometries. Blue circles indicate the possible reflection locations along each surface. The point along a surface with the smallest difference between the angle of incidence and reflection was taken as the path of the reflected transmission.



having no valid reflection geometry for the given tag and receiver combination. Figure 3b shows an example of valid reflection geometries from both surfaces for a given tag and receiver combination.

For all 2000 simulated emissions, PMC-TOA was applied to estimate the tag positions. For each emission, 100 particles were sampled over five iterations of the algorithm. The initial set of proposal location parameters, $\mathbf{M}^{(1)}$, was taken by uniformly sampling along a hexagonal grid within 25 m of any receiver and then emission times were set by solving Equation (4) according to the procedure described earlier. The parameters for the time-of-arrival likelihood were set to fixed values: the direct detection error standard deviation was $\sigma_{\text{det}} = 2$ ms, matching the value used to simulate the data; for the reflected detection error, the maximum reflection latency was $\phi = 200$ ms and shape parameter $\beta = 32$. The value of ϕ was set under the assumption that a transmission will not propagate for more than 300 m and β was arbitrarily chosen to produce a reflection distribution which would not permit large negative detection outliers. The proposal covariance was set to double the value of σ_{det} , giving $\sigma_{\text{prop}} = 4$ ms. The weighted mean of the final sample of particles was taken as the position estimate.

The absolute positioning error was measured by taking the spatial distance between the true location of the simulated tag and the PMC-TOA estimate. The weighted covariance from the PMC-TOA particles was then used to calculate the standardized positioning error. For each position estimate, the Mahalanobis distance (Mahalanobis, 1936) was calculated from the vector of the absolute positioning error and the weighted particle covariance. This was taken as the standardized positioning error. Provided the PMC-TOA algorithm fit well—that is, the distribution of weighted particles resulted in a good approximation to the time-of-arrival likelihood—the standardized positioning errors should fall along a χ_2 distribution. That is, a chi distribution with two degrees of freedom—not to be mistaken for the common chi-squared distribution, χ^2 . Comparing the distribution of these standardized

positioning errors to a χ_2 provides a simple visual indicator for validating the measures of positioning uncertainty returned by PMC-TOA.

For comparison, the absolute and standardized positioning errors were also calculated from TDOA estimated positions. Here, Smith and Abel's (1987) closed form spherical-interpolation method for TDOA positioning was used to estimate the tag positions. The positioning error covariances were then calculated by taking the Jacobian, \mathbf{H} , of the spherical-interpolation solution, giving a matrix of partial derivatives for the estimated x and y coordinates of the tag with respect to the measured detection times. This was used to transform a covariance matrix of detection time errors across all receivers, $\Sigma_{\text{det}} = \mathbf{I} \cdot \sigma_{\text{det}}^2$ where $\sigma_{\text{det}} = 2$ ms and \mathbf{I} is an K by K identity matrix, into an approximation of the spatial positioning error covariance

$$\Sigma_{\text{TDOA}} = \mathbf{H} \cdot \Sigma_{\text{det}} \cdot \mathbf{H}^T. \quad (8)$$

Absolute and standardised position error measures were then calculated with the same method used by the PMC-TOA model.

The TDOA positioning error covariance, as calculated above, is a linear approximation of a non-linear process. It is conditioned on the detection times of ideal direct transmissions. As the detection error increases, the quality of this linear approximation becomes weaker. This difficulty in accurately estimating positioning error without prior knowledge of the true tag location is an inherent weakness of TDOA approaches.

Finally, the capacity for the PMC-TOA model to correctly identify detections resulting from reflected transmissions was examined with a receiver operating characteristic curve. Furthermore, in the subset of simulated data where only one reflection per emission was present, the sensitivity was calculated with respect to the size of the added reflection latency. Here, the additional reflection latency was defined as the difference between the reflected and direct transmission latency, ignoring detection error, for a given tag position and receiver location.

2.3 | Example case study

To demonstrate the real-world utility of the PMC-TOA model, data from three tagged Atlantic salmon smolts was used to observe passage behaviour at the same study site that the simulated arena was based on. Smolts were tracked as they swam downstream past the receiver array. The array was set up to observe route selection: whether smolts would continue downstream into a hydropower intake channel (south) or pass through an open gate in the spillway (south east) (Figure 2). PMC-TOA and TDOA models were used to estimate the tag locations, and Johnson et al.'s (2008) continuous-time correlated random walk (CTCRW) model was applied as a post-processing step to smooth the resulting tracks. Additionally, post-processed PMC-TOA positions were also compared to those fitted by YAPS.

The smolts were released approximately 500m upstream from the spillway between 25 April 2021 and 12 May 2021. An Innovasea V5-1x transmitter (12.7 mm, 0.66 g) was surgically implanted within the inter-peritoneal cavity of each individual. These tags were set to simultaneously emit both *High residency* (HR) and *pulse position modulation* (PPM)—two proprietary formats provided by Innovasea—signals on emission intervals of 2.4 to 2.6 s and 22 to 38 s, respectively. After release, both HR and PPM signals were measured from the passing smolts by a detection array made up of Innovasea HR2-180kHz receivers (Bedford, Nova Scotia, Canada). The study was performed under ethical permission from the Swedish Board of Agriculture (5.8.18-03819/2018).

The time-of-arrival data were pre-processed by correcting for clock drift using a hierarchical mixed model coded in the TMB package in R (Kristensen et al., 2016). Next, the difference-of-arrival values were calculated by subtracting each detection from the first-arriving value for that emission event. Detections with difference values larger than 80 m / 1500 ms⁻¹ were removed from the dataset. This simply removes all detections which have a difference-of-arrival time larger than the size of the receiver array, as these can only result from reflected transmission paths.

Both PMC-TOA and TDOA methods were used to estimate the tag positions and error covariance matrices for all emission events from the three smolts. Here, only emissions with four or more detections were used, as this is necessary for unambiguous position estimates from TDOA methods. The same procedure and parameters were used from the simulated study, except 200 particles were used to fit the PMC-TOA model rather than 100. An examination of sentinel tag detection data—telemetry tags fixed to each receiver with known emission times—suggested that $\sigma_{\text{det}} = 2$ ms was a suitable value for capturing the real direct detection error. Additionally, the sentinel tag data revealed many large positive detection outliers, strongly suggesting the presence of acoustically reflective surfaces in this study site.

After fitting PMC-TOA positions for each fish, the number of detections which likely resulted from reflected transmissions were counted per smolt, where $p_{\text{thresh}} = 0.5$. The position estimates and error covariance matrices were then passed to Johnson

et al.'s (2008) CTCRW model to generate smoothed tracks. The CTCRW model sets restrictions on the tagged animals turning angles and step lengths by treating its instantaneous velocity as an Ornstein-Uhlenbeck process. Here, the CTCRW model was implemented as a Kalman filter in two-dimensional space, as described in Johnson et al. (2008). The positioning error covariance returned from the PMC-TOA and TDOA models were used as observation error matrices and the Ornstein-Uhlenbeck process parameters were set to $\beta = -\log(0.05) \cdot t_{05}^{-1} \text{ s}^{-1}$ and $\alpha = \psi \cdot \sqrt{2\beta} \text{ ms}^{-3/2}$, where $t_{05} = 5$ s and $\psi = 0.2 \text{ ms}^{-1}$. t_{05} and ψ can be interpreted as the time interval required for the velocity correlation to fall below 0.05 and the mode of the stationary velocity magnitude distribution in 2D space, respectively. After applying the Kalman filter, estimates were further refined with a Rauch-Tung-Striebel smoother (Rauch et al., 1965). Finally, positioning uncertainty was reported by calculating 95% confidence ellipses from the positioning error covariance matrices returned by the CTCRW model.

YAPS (version 1.2.5 from CRAN) was also applied to the time-of-arrival dataset for comparison. Here, all emissions with at least three detections were used for positioning. YAPS treated the emission schedule as a random-burst interval where the minimum emission interval was 0 s and the maximum was set to the largest difference between the first-arriving detections for each emission. Additionally, YAPS provides three available detection error distributions: Gaussian, t, or a mixture of the two. In preliminary testing, Gaussian or t distributions gave poor fits, so the mixture option was used. Finally, YAPS uses randomized starting locations when fitting the tracks. Hence, running YAPS multiple times can result in different results; this was observed when fitting the case study dataset. Before each fit, the random seed was set to 1 and that result was presented, allowing for a reproducible analysis.

3 | RESULTS

Figure 4a shows the results for the absolute positioning error analysis on the simulated dataset—distances between the true and estimated tag positions. When no reflections were present, both PMC-TOA and TDOA approaches resulted in comparable absolute positioning errors. When any number of reflections were present, TDOA positioning gave much larger positioning errors. For the PMC-TOA model, increasing reflections resulted in a smaller, more gradual increase in positioning error.

When examining the standardized positioning error in Figure 4b, PMC-TOA provided more accurate measures of positioning uncertainty than TDOA positioning. When any reflections were present, TDOA positioning greatly overshoot the ideal χ_2 distribution. The PMC-TOA method, on the other hand, matched well with the χ_2 distribution, including when a small number of reflections were present. This indicates PMC-TOA is capable of giving reliable estimates of positioning accuracy, particularly when few reflections are present.

The capacity of PMC-TOA to correctly identify detections resulting from reflected transmissions is illustrated in Figure 5. As the

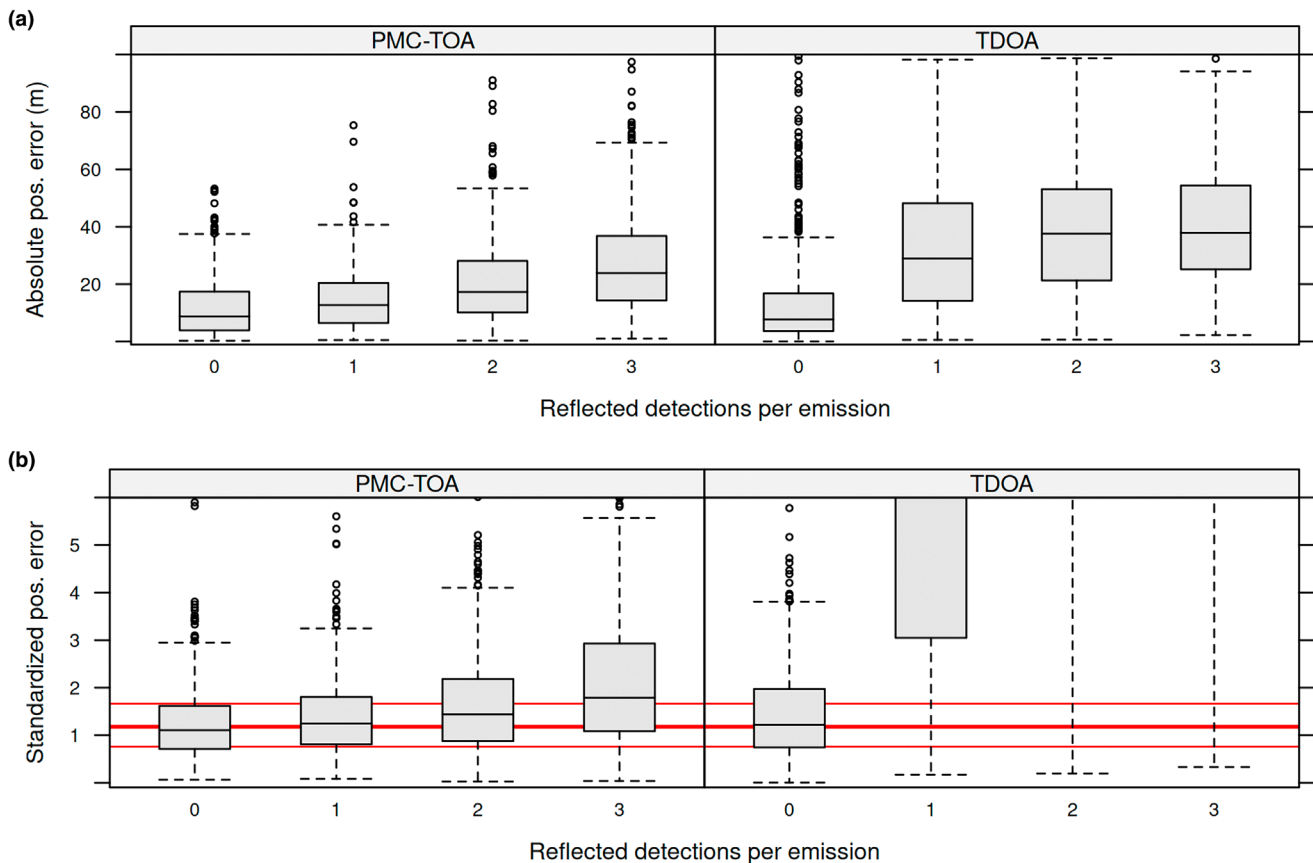


FIGURE 4 Results of fitting the PMC-TOA model to 500 simulated tag emissions per reflection scenario: 0, 1, 2, or 3 reflections per tag emission. Results from TDOA positioning are shown for comparison. Panel (a) shows the absolute positioning error—distance between true and estimated positions. Panel (b) gives the standardized positioning errors, where red lines note the Q1, Q2, and Q3 quartiles of a reference χ^2 distribution. When the model accurately estimates positioning uncertainty, these standardized positioning errors will fall along a χ^2 distribution and the box plot quartiles will align with the red marks.

threshold for marking reflected detections, p_{threshr} decreased from 0.99 to 0.5, the model maintained a very high specificity where rates of direct transmissions being incorrectly marked as reflected remained below 0.04 across all reflection scenarios.

The ability of PMC-TOA to correctly mark reflected transmissions was further examined with respect to the size of the additional reflection latency in the case where only one reflection was present per emission (Figure 6). Unsurprisingly, larger added reflection latencies resulted in higher sensitivities. Very late arriving reflected transmissions, which had an added latency of over 16 ms, were almost always correctly classified.

The case study compared PMC-TOA, TDOA, and YAPS positioning when applied to real tracking data from downstream migrating smolts. The PMC-TOA and TDOA position estimates are plotted alongside the resulting smoothed tracks returned from the CTCRW post-processing model (Figure 7). The resulting tracks from YAPS are shown in Figure 8. In the case study comparison, the true location of the tagged fish is not known. However, the tagging was done during the downstream migration phase for these smolts, and tagged animals were expected to be observed swimming southward along with the water currents, with tracks expected to end in either the turbine intake or the spillway gate areas.

TDOA positions gave tracks starting inside the array and gave erratic movements with no clear heading. PMC-TOA, on the other hand, resulted in tracks that started upstream of the array and exited downstream, in alignment with the expected trajectories. YAPS produced tracks with more erratic movement patterns than PMC-TOA, but broadly followed the expected downstream movements. For fish 3, YAPS expressed a transient jump in the track, likely resulting from a reflected detection incorrectly treated as a direct transmission. For all YAPS fits, the optimizer failed to completely converge. As a result, no error measures were produced for YAPS fits and no confidence ellipses could be plotted.

4 | DISCUSSION

The results from the simulated study showed that PMC-TOA performs comparably to TDOA positioning when no reflected transmissions are present. When reflected transmissions are present, PMC-TOA is often able to identify the resulting detection outliers with an extremely high specificity and return position estimates with only a small decrease in positioning accuracy. Importantly—and unlike TDOA positioning methods—PMC-TOA provides good measures of

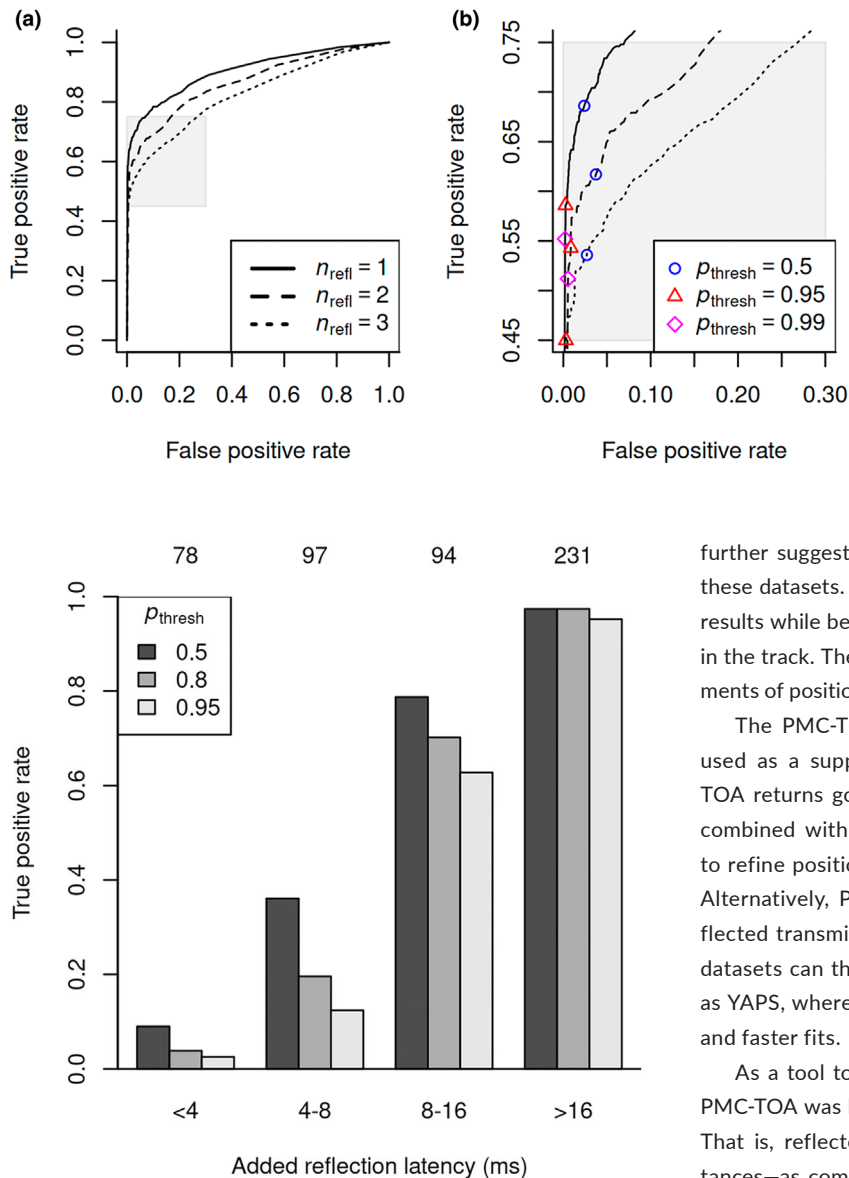


FIGURE 6 The sensitivity of the PMC-TOA model when marking reflected transmissions in a subset of the simulated study where only one reflection is present per emission ($n = 500$). Bars show the rates for three classification thresholds. The x-axis is grouped by the known added reflection latency and the number of emissions per group are shown above the plot. Longer reflected transmission paths, resulting in greater additional reflection latencies, are more readily identified as reflections by PMC-TOA.

positioning uncertainty even when reflections are present. The utility of these uncertainty measures is exemplified in the case study where they were passed to Johnson et al.'s (2008) CTCRW model as a post-processing step. The post-processed tracks resulting from PMC-TOA were vastly different than those from TDOA. When examining the TDOA results—where positioning uncertainty measures are expected to be poor—smolt movements were modelled as erratic paths with no clear heading. On the other hand, the smoothed PMC-TOA tracks suggested smolts 1 and 3 swam downstream past the spillway while smolt 2 passed through the spillway gate. The PMC-TOA model

FIGURE 5 The capacity of the PMC-TOA model to correctly distinguish detections resulting from direct and reflected transmissions in the simulated study. Panel (a) gives the receiver operating characteristic curve for 3 of the reflection scenarios: 1, 2 or 3 reflections per emission (500 emissions each). Panel (b) shows a magnified region of (a) where p_{thresh} values of 0.5, 0.95 and 0.99 have been annotated along each curve.

further suggested that many reflected detections were present in these datasets. YAPS gave similar paths to the smoothed PMC-TOA results while being more erratic and with occasional transient jumps in the track. These tracks, however, were unable to return measurements of positioning uncertainty due to poor convergence.

The PMC-TOA model presented here is recommended to be used as a supplement for other positioning methods. As PMC-TOA returns good measures of positioning uncertainty, it can be combined with state-space models which utilize these measures to refine position estimates—as shown in the case study example. Alternatively, PMC-TOA can be used to identify and remove reflected transmissions from time-of-arrival datasets. These filtered datasets can then be passed on to other positioning models, such as YAPS, where the reduction in large outliers may result in better and faster fits.

As a tool to identify reflected transmissions, the sensitivity of PMC-TOA was largely correlated with the added reflection latency. That is, reflected transmissions that had much longer travel distances—as compared to the direct path between the tag/receiver pair—were more readily marked. As small added reflection latencies will have relatively lower impacts on positioning accuracy, failing to remove them from time-of-arrival datasets may result in a negligible impact on positioning accuracy.

The performance of PMC-TOA is affected by the choice of the algorithm's parameters. Sensible parameters for the time-of-arrival likelihood can be set a priori by examining sentinel tag data from the study site. Additionally, the initial locations for the proposal densities can be uniformly sampled from locations near or within the telemetry array. Values for the number of particles, N , and the proposal standard deviation, σ_{prop} , however, are more challenging to determine and can vary per study site.

Lower values of σ_{prop} along with higher N can more densely sample from the time-of-arrival likelihood, giving better positioning accuracy. However, if σ_{prop} is too low or there are too few particles, the algorithm will return inconsistent and inaccurate position and covariance estimates—an artefact of sample impoverishment. A heuristic approach for choosing these values is to repeatedly apply PMC-TOA to the same time-of-arrival data with initial high

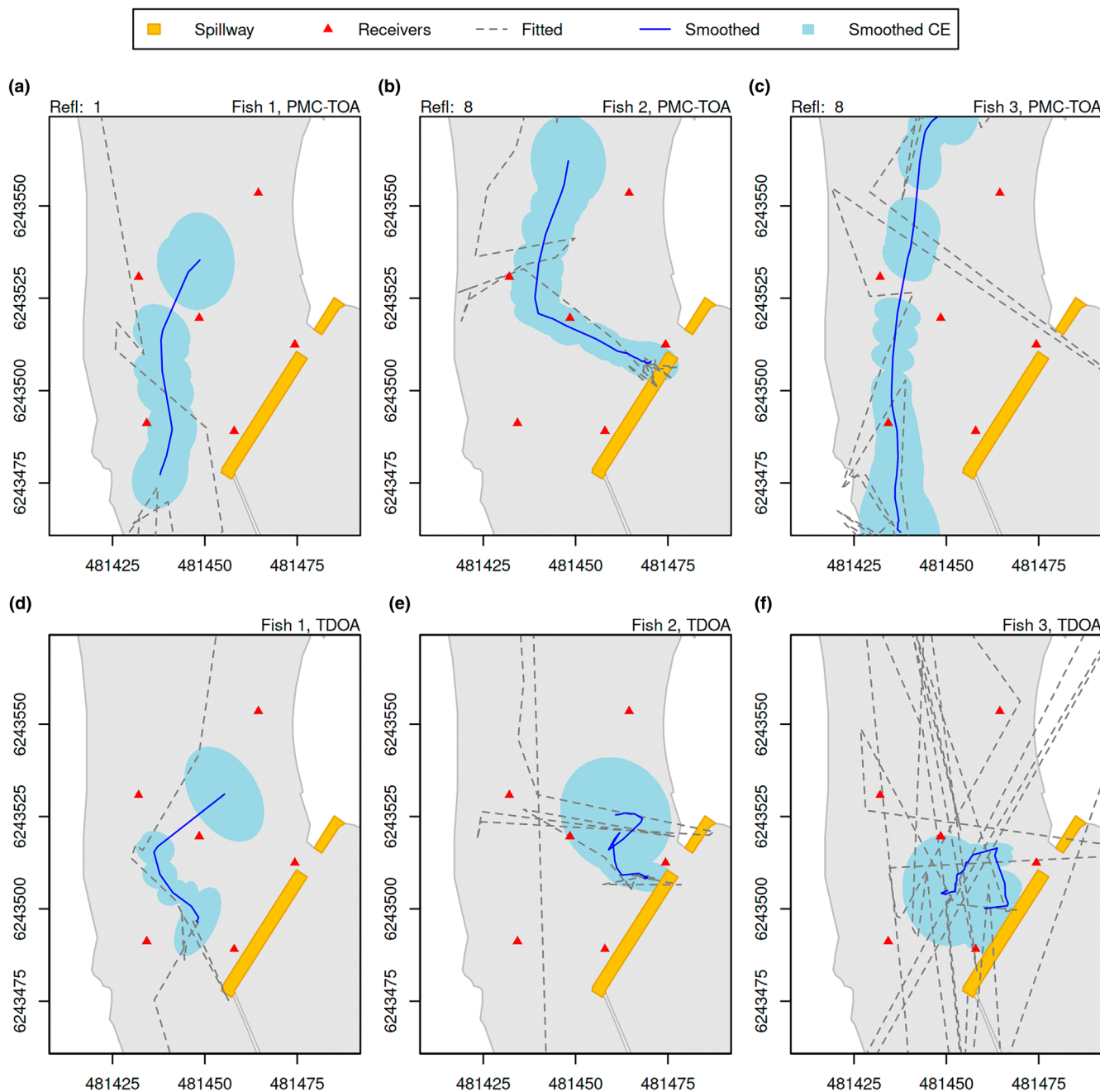


FIGURE 7 A comparison of PMC-TOA (a–c) and TDOA (d–f) tracks fitted to the real case study data where emissions had at least four detections. The fitted tracks from both models are given by dashed lines and the smoothed tracks from post-processing with the CTCRW model are shown in blue. The 95% confidence ellipses for the post-processed point estimates are shown as light blue polygons and the number of likely reflections estimated by PMC-TOA are noted in the top margins (detections with $p_k \geq 0.5$). Coordinate reference system: WGS84/UTM Zone 33N.

values for both σ_{prop} and N . These parameters can be gradually lowered until a high and consistent positioning accuracy is attained.

In the simulated study, positions were solved at rate of 18 per second when using 100 particles (Intel i5-13600K CPU, code written in R). While setting a high number of particles can both improve positioning accuracy and the stability of the algorithm, it comes at the cost of increased processing times. PMC-TOA calculates the particle weights in Equation (2) according to the deterministic mixture

PMC algorithm from Elvira et al. (2017). Here, the weight of each particle is evaluated by averaging across the entire set of N proposal densities within that iteration. As a result, increasing the number of particles may lead to an exponential increase in processing times.

For study areas containing large telemetry arrays, a high number of particles may be required to avoid sample impoverishment. In these cases, the standard PMC weighting approach from Cappé et al. (2004) can instead be used where

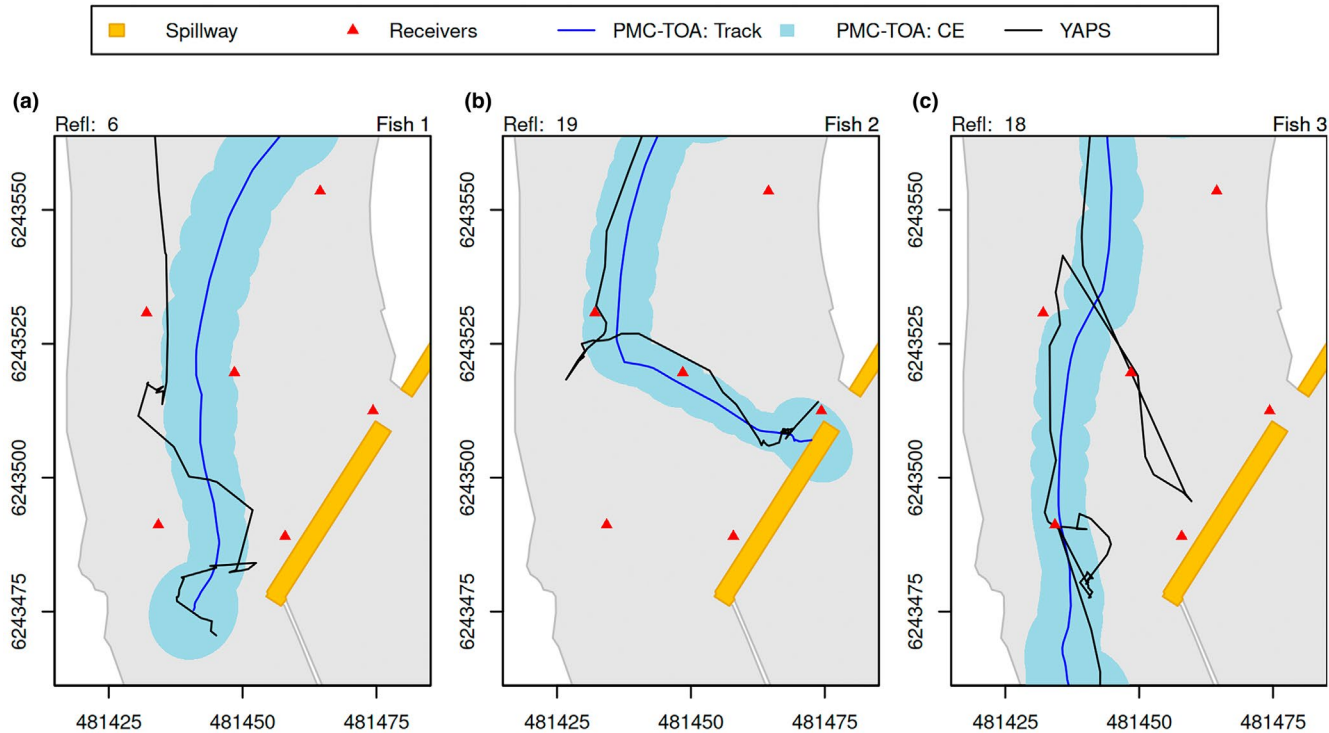


FIGURE 8 A comparison of YAPS and post-processed PMC-TOA tracks fitted to the case study dataset where emissions had at least three detections (panels a-c). The 95% confidence ellipses for the post-processed PMC-TOA estimates are shown as light blue polygons and the number of likely reflections estimated by PMC-TOA are noted in the top margins (detections with $p_k \geq 0.5$). Note that no confidence intervals are shown for YAPS positions as all fits failed to fully converge. Coordinate reference system: WGS84/UTM Zone 33N.

$$w_i^{(g)} = \frac{\mathcal{L}(\mathbf{x}_i^{(g)} | \mathbf{y})}{q(\mathbf{x}_i^{(g)} | \boldsymbol{\mu}_i^{(g)})}. \quad (9)$$

Here, each particle is only evaluated at the proposal location from which it was sampled. As a result, computation times are much shorter and are expected to scale linearly with the volume of particles at the cost of lower performance per particle. For further decreases to processing times, the number of iterations, G , can also be reduced. In both the simulated and case studies, five iterations were run, although good position estimates generally appeared to result from as few as three in this particular setup.

For very large study areas with many receivers, the time-of-arrival likelihood used by PMC-TOA can be implemented within a particle filter framework. Particle filters may be more suitable in these contexts, as the locations of the initial proposal distributions $M^{(1)}$ for a given emission are sampled from predictions conditioned on the previous emission's location and time estimates. In practice, this means that fewer particles are required, as the initial proposal distributions cover a much smaller and important space. Particle filters have recently been shown as a promising tool for tracking animals through telemetry arrays (Lavender et al., 2023, 2024).

In the case study comparison, YAPS yielded tracks that broadly followed the same path as the smoothed estimates from PMC-TOA. Here, YAPS showed more movement jitter, an expected result of the Gaussian random walk utilized as an animal movement model. A caveat, however, is that YAPS's consistency failed to converge on our

case study dataset. In addition to providing no estimates of positioning uncertainty, reapplying YAPS would result in notably different tracks. This is on account of the randomized initial values YAPS passes to the optimizer. For challenging datasets such as this case study, YAPS may require either good starting values or it must be rerun when the resulting tracks are judged to be poor. For fish 3, when YAPS was repeatedly applied with different random seeds, the large transient jump in the track—clearly deviating from PMC-TOA's estimates—was randomly present.

On a final note, telemetry arrays have unique spatial and temporal patterns of detection and positioning error. As a result, it is particularly challenging to describe the sensitivity of a given positioning model in a manner that is broadly applicable to the diversity of array set-ups deployed in practice. Moreover, pre-processing actions applied to time-of-arrival datasets—such as clock drift correction—have a large effect on the quality of the resulting position estimates. Within the acoustic telemetry community, there is a need for a collection of benchmark datasets where positioning models can be compared against each other. Ideally, this should include a mixture of both GPS-truthed tracking data and simulated movement tracks, along with a variety of pre-processing methods and study environments. With such a benchmark dataset to compare against, researchers may have more realistic expectations on how well a particular positioning model may perform within their array set-up.

As telemetry positioning arrays are increasingly being deployed in areas near reflective structures, PMC-TOA provides a fast positioning algorithm that can handle reflected transmissions. Moreover,

even in the case where no reflected transmissions are present, PMC-TOA provides good measures of positioning uncertainty, which can be utilized by post-processing state-space models to give accurate movement tracks of tagged animals. Utilized for either pre-processing or positioning, PMC-TOA is a useful tool for researchers interested in fine-scale telemetry positioning.

AUTHOR CONTRIBUTIONS

James Adam Campbell developed the model, executed the analysis and wrote the manuscript and [Supporting Information](#). Samuel Joseph Shry and Olle Calles collected and curated the case study dataset. Samuel Joseph Shry and Petter Lundberg reviewed the [Supporting Information](#). All authors reviewed and contributed to the manuscript.

ACKNOWLEDGEMENTS

This project has received funding from the following: European Union Horizon 2020 Research and Innovation Programme under the Marie Skłodowska-Curie Actions, grant agreement no. 860800; Uniper/Sydkraft Hydropower AB; Stiftelsen för Kunskaps- och Kompetensutveckling, grant number: 20160160; and EU-LIFE Program, grant number: LIFE18 NAT/SE/000742. Open Access funding enabled and organized by Projekt DEAL.

CONFLICT OF INTEREST STATEMENT

The named authors declare no conflict of interest, financial or otherwise.

PEER REVIEW

The peer review history for this article is available at <https://www.webofscience.com/api/gateway/wos/peer-review/10.1111/2041-210X.14508>.

DATA AVAILABILITY STATEMENT

All R code and data used to generate the figures and results are available via <https://doi.org/10.5281/zenodo.14719265> (Campbell et al., 2025).

ORCID

James Adam Campbell  <https://orcid.org/0000-0002-6150-0821>

Petter Lundberg  <https://orcid.org/0000-0003-3481-5163>

REFERENCES

- Ainslie, M. (2010). *Principles of sonar performance modelling*. Springer.
- Baktoft, H., Gjelland, K. Ø., Økland, F., & Thygesen, U. H. (2017). Positioning of aquatic animals based on time-of-arrival and random walk models using yaps (yet another positioning solver). *Scientific Reports*, 7(1), 14294.
- Bucker, H. P. (1964). Normal-mode sound propagation in shallow water. *The Journal of the Acoustical Society of America*, 36(2), 251–258.
- Campbell, J., Shry, S. J., Lundberg, P., Calles, O., & Hölker, F. (2025). A population monte carlo model for underwater acoustic telemetry positioning in reflective environments: Analysis data and code. *Zenodo* <https://doi.org/10.5281/zenodo.14719265>
- Cappé, O., Guillin, A., Marin, J. M., & Robert, C. P. (2004). Population monte carlo. *Journal of Computational and Graphical Statistics*, 13(4), 907–929.
- Elvira, V., Martino, L., Luengo, D., & Bugallo, M. F. (2017). Improving population monte carlo: Alternative weighting and resampling schemes. *Signal Processing*, 131, 77–91.
- Ingraham, J. M., Deng, Z. D., Li, X., Fu, T., McMichael, G. A., & Trumbo, B. A. (2014). A fast and accurate decoder for underwater acoustic telemetry. *Review of Scientific Instruments*, 85(7), 074903.
- Johnson, D. S., London, J. M., Lea, M.-A., & Durban, J. W. (2008). Continuous-time correlated random walk model for animal telemetry data. *Ecology*, 89(5), 1208–1215.
- Kjærås, H., Baktoft, H., Silva, A. T., Gjelland, K. Ø., Økland, F., Forseth, T., Szabó-Mészáros, M., & Calles, O. (2023). Three-dimensional migratory behaviour of European silver eels (*Anguilla Anguilla*) approaching a hydropower plant. *Journal of Fish Biology*, 102(2), 465–478.
- Kristensen, K., Nielsen, A., Berg, C. W., Skaug, H., & Bell, B. M. (2016). Tmb: Automatic differentiation and Laplace approximation. *Journal of Statistical Software*, 70(5), 1–21.
- Lavender, E., Biber, S., Illian, J., James, M., Wright, P. J., Thorburn, J., & Smout, S. (2023). An integrative modelling framework for passive acoustic telemetry. *Methods in Ecology and Evolution*, 14(10), 2626–2638.
- Lavender, E., Scheidegger, A., Albert, C., Biber, S. W., Illian, J., Thorburn, J., Smout, S., & Moor, H. (2024). pater: Particle algorithms for animal tracking in r and julia. *bioRxiv*.
- Lennox, R. J., Aarestrup, K., Alós, J., Arlinghaus, R., Aspillaga, E., Bertram, M. G., Birnie-Gauvin, K., Brodin, T., Cooke, S. J., Dahlmo, L. S., Dhellemmes, F., Gjelland, K. Ø., Hellström, G., Hershey, H., Holbrook, C., Klefoth, T., Lowerre-Barbieri, S., Monk, C. T., Nilsen, C. I., ... Baktoft, H. (2023). Positioning aquatic animals with acoustic transmitters. *Methods in Ecology and Evolution*, 14(10), 2514–2530.
- Mahalanobis, P. C. (1936). On the generalised distance in statistics. *Proceedings of the National Academy of Sciences, India*, 2, 49–55.
- Nadarajah, S. (2005). A generalized normal distribution. *Journal of Applied Statistics*, 32(7), 685–694.
- Rauch, H. E., Tung, F., & Striebel, C. T. (1965). Maximum likelihood estimates of linear dynamic systems. *AIAA Journal*, 3(8), 1445–1450.
- Smith, J., & Abel, J. (1987). Closed-form least-squares source location estimation from range-difference measurements. *IEEE Transactions on Acoustics, Speech, and Signal Processing*, 35(12), 1661–1669.
- Trancart, T., Carpentier, A., Acou, A., Danet, V., Elliott, S., & Feunteun, E. (2020). Behaviour of endangered european eels in proximity to a dam during downstream migration: Novel insights using high accuracy 3D acoustic telemetry. *Ecology of Freshwater Fish*, 29(2), 266–279.
- Vergeynst, J., Vanwyck, T., Baeyens, R., De Mulder, T., Nopens, I., Mouton, A., & Pauwels, I. (2020). Acoustic positioning in a reflective environment: Going beyond point-by-point algorithms. *Animal Biotelemetry*, 8(1), 16.

SUPPORTING INFORMATION

Additional supporting information can be found online in the Supporting Information section at the end of this article.

Supporting Information S1. Example implementation in R.

Data S1

How to cite this article: Campbell, J. A., Shry, S. J., Lundberg, P., Calles, O., & Hölker, F. (2025). A population Monte Carlo model for underwater acoustic telemetry positioning in reflective environments. *Methods in Ecology and Evolution*, 16, 775–785. <https://doi.org/10.1111/2041-210X.14508>